NeuroImage 223 (2020) 117344

Contents lists available at ScienceDirect

NeuroImage

journal homepage: www.elsevier.com/locate/neuroimage

Localization of deep brain activity with scalp and subdural EEG

Mansoureh Fahimi Hnazaee[a,*], Benjamin Wittevrongel[a], Elvira Khachatryan[a], Arno Libert[a], Evelien Carrette[b], Ine Dauwe[b], Alfred Meurs[b], Paul Boon[b], Dirk Van Roost[b], Marc M. Van Hulle[a]

[a] Laboratory for Neuro- and Psychophysiology, Department of Neurosciences, KU Leuven, Belgium
[b] Faculty of Medicine and Health Sciences, Ghent University Hospital, Ghent, Belgium

ARTICLE INFO

Keywords:
Joint EEG
ECoG
Depth electrode
Source localization
Quiet wakefulness
Deep brain activity

ABSTRACT

To what extent electrocorticography (ECoG) and electroencephalography (scalp EEG) differ in their capability to locate sources of deep brain activity is far from evident. Compared to EEG, the spatial resolution and signal-to-noise ratio of ECoG is superior but its spatial coverage is more restricted, as is arguably the volume of tissue activity effectively measured from. Moreover, scalp EEG studies are providing evidence of locating activity from deep sources such as the hippocampus using high-density setups during quiet wakefulness. To address this question, we recorded a multimodal dataset from 4 patients with refractory epilepsy during quiet wakefulness. This data comprises simultaneous scalp, subdural and depth EEG electrode recordings. The latter was located in the hippocampus or insula and provided us with our "ground truth" for source localization of deep activity. We applied independent component analysis (ICA) for the purpose of separating the independent sources in theta, alpha and beta frequency band activity. In all patients subdural- and scalp EEG components were observed which had a significant zero-lag correlation with one or more contacts of the depth electrodes. Subsequent dipole modeling of the correlating components revealed dipole locations that were significantly closer to the depth electrodes compared to the dipole location of non-correlating components. These findings support the idea that components found in both recording modalities originate from neural activity in close proximity to the depth electrodes. Sources localized with subdural electrodes were ~70% closer to the depth electrode than sources localized with EEG with an absolute improvement of around ~2cm. In our opinion, this is not a considerable improvement in source localization accuracy given that, for clinical purposes, ECoG electrodes were implanted in close proximity to the depth electrodes. Furthermore, the ECoG grid attenuates the scalp EEG, due to the electrically isolating silastic sheets in which the ECoG electrodes are embedded. Our results on dipole modeling show that the deep source localization accuracy of scalp EEG is comparable to that of ECoG.

Significance Statement

Deep and subcortical regions play an important role in brain function. However, as joint recordings at multiple spatial scales to study brain function in humans are still scarce, it is still unresolved to what extent ECoG and EEG differ in their capability to locate sources of deep brain activity. To the best of our knowledge, this is the first study presenting a dataset of simultaneously recorded EEG, ECoG and depth electrodes in the hippocampus or insula, with a focus on non-epileptiform activity (quiet wakefulness). Furthermore, we are the first study to provide experimental findings on the comparison of source localization of deep cortical structures between invasive and non-invasive brain activity measured from the cortical surface.

2. Introduction

How accurately source signals from deep and subcortical regions can be localized using electrophysiological recordings from the human cortical surface is still under debate. The uncertainty partly stems from the fact that these structures have a distinct neuronal architecture which may cause them to produce weaker signals in comparison to cerebral structures (Andersen et al., 2020, Attal and Schwartz, 2013; da Silva and Lopes, 2011). Moreover, compared to cortical activity, the larger distance to deep structures attenuates the recorded electrode activity (Krishnaswamy et al., 2017). Recordings from the cortical surface are predominantly done using non-invasive electrophysiological tools such as magneto- and electroencephalography ((M)EEG). For certain clinical purposes, invasive cortical recordings are also done with

* Corresponding author.
E-mail address: mansoureh.fahimihnazaee@kuleuven.be (M. Fahimi Hnazaee).

https://doi.org/10.1016/j.neuroimage.2020.117344
Received 19 February 2020; Received in revised form 27 July 2020; Accepted 31 August 2020
Available online 6 September 2020

electrocorticography (ECoG). ECoG has a considerable advantage over (M)EEG in locating proximal activity, as the recordings are not spatially filtered or "blurred" by the cranium. However, ECoG grids or strips typically only cover a restricted region of the cortical surface compared to the whole scalp coverage of (M)EEG, which is expected to affect localization accuracy of more distal sources. Therefore, to date, it is unclear whether ECoG has an edge over (M)EEG when it comes to localizing source signals from deep and subcortical regions.

In (M)EEG studies, high-density settings have successfully localized activity directly recorded from the hippocampus, amygdala, thalamus and nucleus accumbens (Pizzo et al., 2019, Seeber et al., 2019). The importance of these two findings has been emphasized recently (da Silva (da Silva and Lopes, 2019)) as it challenges the assumption that activity from small and deep/subcortical structures does not have sufficient signal-to-noise ration to be reliably detected without the need for excessive averaging (Puce and S. Hämäläinen, 2017). When the ground truth is available, as is the case with these studies, by virtue of depth electrodes, source separation and localization techniques can be correctly assessed in their ability to gauge the activity of the mentioned deep structures. The studies by Pizzo et al. and Seeber et al. are not the first ones advocating the detectability of subcortical structures in (M)EEG. In fact, there has since long been a steady flow of either theoretical or experimental studies to support this claim (Cebolla et al., 2016; Cosandier-rimélé et al., 2012; Daly et al., 2019; Dumas et al., 2013; Gharib et al., 1995; Ruzich et al., 2019; Samuelsson et al., 2019; Scherg and Von Cramon, 1985; Schoffelen et al., 2008; Tzovara et al., 2019). Simultaneous (M)EEG and deep electrode recordings have shown to share remarkably similar properties (Dalal Sarang et al., 2009, Dubarry et al., 2014, Litvak et al., 2010, Tonoyan et al., 2017), though these findings have been fairly limited to clinical settings (Koessler et al., 2015; Ramantani et al., 2016). Especially of interest to this study is EEG and EEG source modeling, which requires a much more complex model considerably affected by the conductivity properties of the different tissues of the head (Puce and S. Hämäläinen, 2017). Advances in the last decades on the detectability and localization of subcortical and deep structures have gone hand in hand with improvements in spatial resolution of EEG, now down to millimeter-scale when using high-density settings and in EEG source reconstruction techniques (Grech et al., 2008, Marinazzo et al., 2019; Pascual-Marqui, 1999).

Invasive measures of electrophysiological activity such as ECoG, by contrast, are hailed for their superior spatial resolution, spectral bandwidth and signal-to-noise ratio (SNR) compared to scalp electrode recordings (Ball et al., 2009). The spatial distribution of ECoG potentials is complex (Whitmer et al., 2010) and the presence of highly localized components (e.g. high-gamma band during a visual task (Wittevrongel et al., 2018)) has led researchers to claim that ECoG is a local signal (Dubey X and Supratim Ray, 2019). This locality principle predicts that only sources directly underneath and well-covered by the subdural grid can be reconstructed successfully. An advantage of having a more restricted volume of sensitivity is that it reduces the amount of surrounding background activity captured by the electrodes (Cosandier-rimélé et al., 2012). Therefore, adding more subdural grids for the purpose of source localization might even decrease SNR if the extra contacts are not close enough to the source. Some studies show the source localization accuracy of activity with ECoG decreases linearly with the distance from the electrodes (Todaro et al., 2019, Zhang et al., 2008). However, studies have applied signal separation techniques and observed that signals from subdural grids or strips may also detect activity from more distal sources (Whitmer et al., 2010). It should be noted that, in contrast to (M)EEG, the used localization methods for ECoG are typically based on activity from a single or a small group of adjacent cortical electrodes (Huiskamp, 2002). More advanced methods for source reconstruction, such as the dipole equivalent and distributed source models, are not systematically applied nor optimized for ECoG source localization purposes (Pascarella et al., 2016), despite evidence of increased model accuracy ((Dümpelmann et al., 2009); Oostenveld and (Oostenveld and F. Oostendorp, 2002; Todaro et al., 2019)) and significant improvements in deep source identification (Cho et al., 2011).

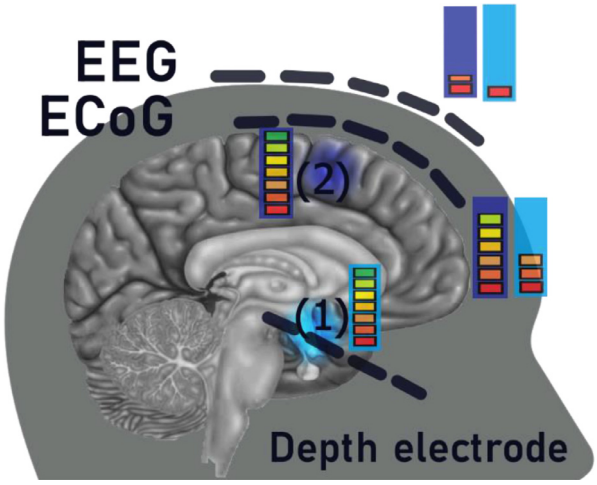

Fig. 1. Schematic overview of the study. Deep and superficial are located at locations (1) and (2), respectively. The color bars indicate the measurement strength of the source activity when measured at the origin of the source (maximum strength) and with ECoG or EEG electrodes. Light blue and dark blue represent the measured strength for deep and superficial sources, respectively. The measurement of deep and superficial sources are attenuated at both subdural and scalp level but to a different extent. From a perspective of the scalp (EEG), attenuation is likely so strong that the SNR for deep and superficial sources do not differ as much as they do from a subdural perspective (ECoG). This could partially explain why source localization accuracy of deep sources with ECoG is comparable with that of EEG (see discussion). Note that only the level of attenuation is relevant, not the extent of the spread or location of the observed activity.

To assess how in practice EEG and ECoG compare in terms of deep source localization requires simultaneous recordings of invasive, non-invasive cortical and deep activity. Fig. 1 gives a schematic overview of such a study. Simultaneous invasive and non-invasive recordings to isolate the contributions of the underlying neural activity to EEG have been primarily studied in nonhuman primates (Musall et al., 2014; Snyder et al., 2018). But these results do not necessarily generalize to human data as the properties of the skull, shape and cancelation properties of the cortical and subcortical structures may differ substantially. In human studies, simultaneous recordings have been performed in clinical settings to determine the amplitude and extent of cortical activation that determines the presence of cortical spikes in scalp EEG (Abraham and Ajmone Marsan, 1958. Cosandier-rimélé et al., 2012. Ramantani et al., 2016). Outside of the clinical context, human studies have found a high correlation between ECoG and EEG for a given task (Ball et al., 2008. Haufe et al., 2018), although these studies did not consider simultaneously recorded ECoG and EEG as it is not without obstacles (Dubarry et al., 2014). Hence, a study comparing source localization of both modalities within the same subject would be of great significance to the field (Nunez Paul et al., 2019).

To fill this gap, we recorded electrophysiological activity from 4 patients during quiescent wakefulness simultaneously from depth electrodes implanted in the hippocampus or insula, subdural grids covering the cortical surface closest to these depth electrodes and scalp EEG electrodes. We recorded these patients during quiescent wakefulness as a focus on non-epileptiform electrophysiological activity in human studies outside the context of task-related responses is still relatively scarce (Frauscher et al., 2018). Source separation using ICA was performed separately on the scalp- and subdural electrodes. Several studies support the notion that independent components of EEG correspond to an equivalent dipole, i.e. a maximally independent component represents a stationary source (Delorme et al., 2012). Additionally, the use of ICA

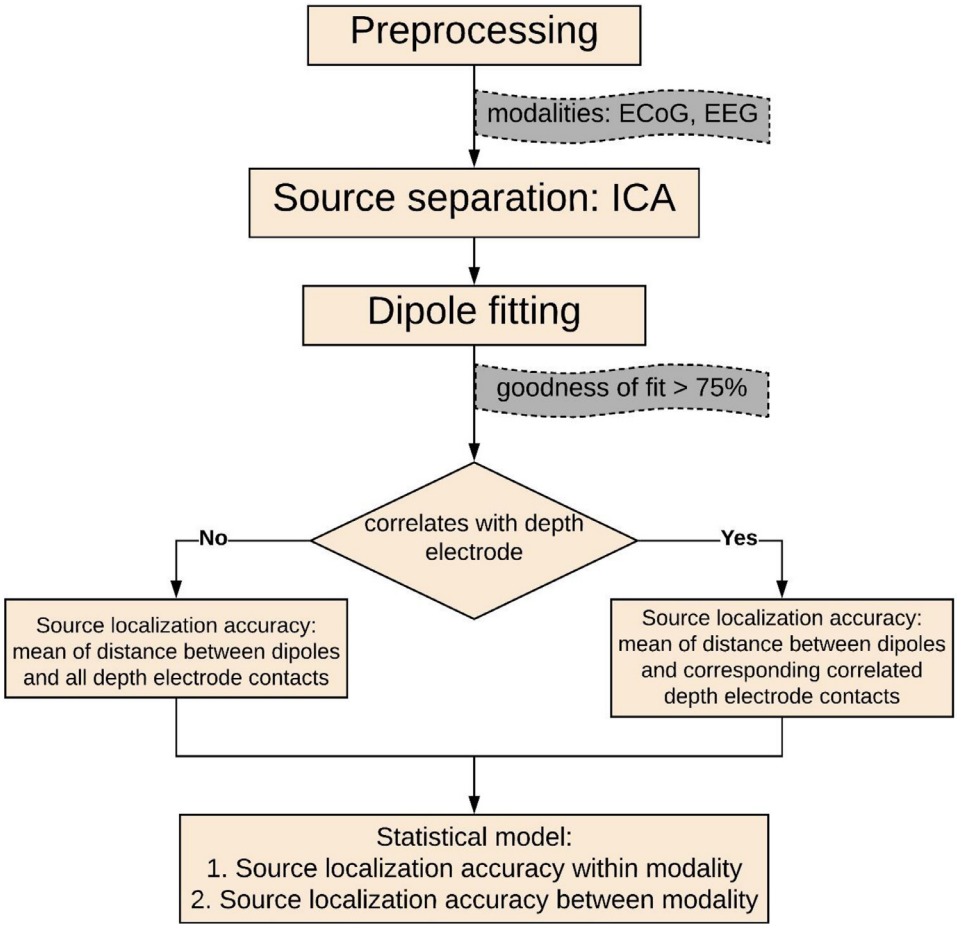

Fig. 2. Block diagram of the pipeline used to investigate source localization accuracy within and between modalities.

for intracranial data has been studied, where it was also shown that several IC projections are consistent with sources from single brain regions (Whitmer et al., 2010). Based on these studies, we assumed that the topographic map of each subdural or scalp IC component corresponds to a single dipole and performed dipole modeling to locate the generator of each of these component topographies. The distance between the estimated generator and the depth electrodes was computed. In this way, we were able to evaluate and compare the source reconstruction of the scalp- and subdural electrodes, given the same deep source activity as identified by the depth electrodes (see Fig. 1).

3. Materials and methods

Fig. 2 shows an overview of the pipeline used in our study which consists of several steps.

3.1. Participants

We recorded simultaneous depth electrode, ECoG and (scalp) EEG from 4 patients (2 females, average age 41.5 y std=20 y, 2 left-handed) with drug-resistant focal epilepsy and undergoing pre-surgical clinical assessment. All patients had normal vision and normal levels of consciousness. The study was conducted according to the current version of the declaration of Helsinki, following ethical approval from Ghent University Hospital's Ethics Committee. All patients gave their written informed consent before participating in the study.

3.2. Data acquisition

EEG was recorded from 27 active electrodes attached to the scalp according to the 10-20 international system. In addition to the scalp electrodes, patients had been implanted with both depth and subdural platinum electrodes embedded in silastic (Ad-Tech, USA) for invasive video EEG monitoring at Ghent University Hospital. For the subdural grids, contact diameter was 4 mm with an exposure of 2.3 mm diameter and a center-to-center distance of 10 mm; the depth electrodes had 6 or 8 contacts per electrode with contact size of 2.4/1.1 mm (overall length/diameter) and 4 mm center-to-center distance. All recordings were digitized at a sampling rate of 256 Hz (except for patient P3, where it was 1024Hz) using an SD LTM 64 Express (Micromed, Italy) medically certified device. The number and location of the subdural grids and depth electrodes for each patient are listed in table S1 and figure S1 of the supplementary material section. The table also lists the patients' demographics.

3.3. Experimental procedure

For this study, we recorded each patient's spontaneous activity with eyes open for 3 minutes while they fixated a cross-hair presented on an LCD screen at a distance of approximately 60 cm. Patients were sitting upright in their hospital beds.

3.4. Localization of subdural and depth electrodes

The pre-implantation MRI scan of the patient was used for cortical reconstruction and volumetric segmentation using the Freesurfer image analysis suite ((Dale Anders et al., 1999) version 6.0, see http://surfer.nmr.mgh.harvard.edu/). The Freesurfer output and MRI scan were then loaded into Brainstorm (Tadel et al., 2011), where the MRI was then co-registered with the post-implantation CT scan using the SPM12 extension (https://www.fil.ion.ucl.ac.uk/spm/software/spm12/). The coordinates of the implanted subdural and depth electrodes were obtained

by visual inspection and mapped onto the cortical surface to account for possible post-implantation tissue shifting. The results of the MRI segmentation were further used to create the head model for dipole modeling (see the section on dipole modeling).

3.5. Pre-processing

The raw ECoG, depth electrode and EEG recordings were first inspected for bad channels. In the case of subdural and depth recording, bad channels were identified by a specialized epileptologist (co-author AM) who marked, in addition to the electrodes, also the time intervals during which the recordings exhibited frequent or continuous abnormal activity (interictal or ictal activity and abnormal slowing). These electrodes and time intervals were excluded from our study as well as the corresponding time intervals from the EEG recordings. In principle, we could investigate source reconstruction accuracy of the abnormal activity too, but we decided to exclude it as we wanted the results to be relevant for healthy subjects with normal brain activity. Additionally, depth electrodes were checked for their anatomical location using Brainstorm and when electrode contacts were outside the deep structures (hippocampus for 3 patients, hippocampus and insula for 1 patient), they were discarded from further analysis. The noisy electrodes in EEG were identified using the manual reject function in FieldTrip (Oostenveld et al., 2011). The data was initially filtered using a bandpass filter between 1-60 Hz and re-referenced offline using a common average reference (CAR) per acquisition modality. For the depth electrode data, we additionally re-referenced our recordings to bipolar ones to investigate the impact of depth electrode set-up on our results, as bipolar recordings are assumed to be less sensitive to volume conduction, thus, allowing for a more precise spatial localization of transient events (Pizzo et al., 2019). The bipolar setup consists of subtracting the recording of all pairs of non-rejected consecutive contacts within each electrode (Dubarry et al., 2014). After that, the recordings were cut into overlapping time windows (epochs), shifted by 2sec. This resulted in an average of 67, 59, 51 and 46 (std=22.1, 24.8, 27.3 and 27.9) epochs for window lengths of 5, 10, 15 and 20 seconds, respectively. The whole pipeline analysis is repeated for each window length.

3.6. CA and correlation

Independent component analysis (ICA) was performed on the ECoG and EEG data for each patient separately, using the Icasso package (Himberg et al., 2004) implemented in FieldTrip. Icasso finds more reliable components than those of a single run of an ICA algorithm by rerunning the FastICA algorithm several times (“iterations”) but with slightly different initial conditions and visualizing the clustering structure of the obtained components per iteration in signal space (using a symmetric approach and accounting for Gaussian non-linearity). In our case, we ran the algorithm for 100 iterations. In each iteration, FastICA was performed on the artifact-free epochs in concatenated format. We had sufficient data to perform the analysis since, after exclusion of bad time intervals, we ended up with an average of 41,601 data points, and the number of electrodes ranged from 15-52 even in the worst case the ratio of data points to electrodes was still at least 15 (Delorme and Makeig, 2004). As the number of ICs is equal to the number of input channels, therefore, there were typically more ICs for ECoG than for EEG.

After ICA analysis, the resulting ICs for both ECoG and EEG, in addition to the data from the depth electrodes, were bandpass filtered using a two-pass Butterworth filter of order 4 in three frequency bands, theta (4-8 Hz), alpha (8-12 Hz), and beta (12-28 Hz). These were chosen as they have been shown to correspond to the most dominant frequencies observed in resting-state ECoG (Groppe David et al., 2013). For each of these frequency bands, we obtained the power envelope of the signal using the Hilbert transform. The power envelope for the depth electrode contacts was calculated in the same way. Next, we calculated the Pearson correlation between each output component and all depth electrode contacts for all epochs, resulting in a total of components × depth electrode contacts × epochs correlation values for each frequency band and patient. Aside from correlation analysis between the depth electrode contacts and independent components of the ECoG and EEG, a preliminary correlation analysis was also performed between depth electrode contacts and the power envelope of the original time series of the ECoG and EEG in each of the abovementioned frequency bands (without performing ICA).

3.7. Dipole modeling

Several studies support the notion that independent components of EEG correspond to an equivalent dipole (Delorme et al., 2012). Therefore we will assume that the topographic map of subdural or scalp IC component corresponds to a single dipole (provided that the goodness-of-fit is sufficiently high, see further) and perform dipole modeling on all components using the dipole modeling function provided by the Brainstorm toolbox. In this function, the forward solution is estimated using a realistic three-layer head model (OpenMEEG BEM) were the source space was constrained to the whole MRI volume with 15000 vertices and relative conductivities of 1, 0.0125, 1 for the scalp, skull, and brain layers, respectively (Gramfort et al., 2010). Even though the Brainstorm toolbox allows for a mixed head model which includes deep and subcortical structures, we did not opt for this method as dipole modeling is not available for a mixed head model of ECoG data. Separate head models were created for the ECoG and EEG data, using the individual MRI anatomy of each patient (see section on localization of subdural and depth electrodes). When performing dipole modeling using Brainstorm, a dipole scanning map is produced that represents the ability of the dipole to explain the recordings. The noise covariance matrix was set as the identity matrix and the median eigenvalue used for noise covariance regularization. The subsequent dipole scanning routine determines the final location and orientation of the best fitting dipole (one dipole per IC). Of each obtained dipole, a goodness of fit is returned indicating what percentage of the total variance is explained by the model variance. Another output is “performance”, the square root of the chi-square summing over the degrees of freedom. This value is similar to a z-scoring, therefore, any performance substantially larger than 5 may be thought of as significant (https://neuroimage.usc.edu/brainstorm/Tutorials/TutDipScan). In our analysis, all dipoles with a performance below 100 were discarded and our statistical analysis performed for dipoles with a goodness of fit of 75% or above, as sources with lower goodness of fit were considered as inconclusive for single dipole fit (Pizzo et al., 2019). Different thresholds of goodness-of-fit for the dipoles were evaluated and reported in the supplementary table S6.

We performed dipole modeling and scanning for all resulting components of both ECoG and EEG. We divided all resulting dipoles into two groups; dipoles that correspond to an independent component, exhibiting a significant correlation with a depth electrode contact and those that don’t. We will further refer to these as the correlating and non-correlating dipoles.

3.8. Statistical analysis

Correlations were assessed for significance which is maximal at zero lag using a surrogate dataset. The surrogate dataset was produced by keeping the original order of the epochs in the first group (the epochs of the depth electrode contacts) and a random permutation of the order of the epochs in the second group (the epochs of the EEG or ECoG components, Matlab’s *randperm* function). By doing this one time, we obtained a surrogate dataset with the same size as the original dataset. Correlation values were then calculated for both the surrogate and the original dataset. A one-sided nonparametric permutation test with 1000 permutations confirmed a significantly larger value for the real correlation

values compared to the surrogate ones. The cross-correlation between components and depth electrode contacts that showed significant correlation was further evaluated by testing whether cross-correlation values were maximum at zero-lag, as a maximum at a lag different from zero would probably indicate a phase-delayed connection rather than volume conduction, therefore, these significant values were discarded from further analysis. An example of the cross-correlation function between depth electrode contact and ECoG/EEG components for one patient can be found in supplementary figure S2. Finally, p-values were corrected for multiple comparisons using the false discovery rate (FDR) correction for the number of components.

To assess the accuracy of source localization, we estimated the distance between the independent components and the depth electrode contacts with which they were correlated. This is termed in the study "source localization accuracy," as our hypothesis is that independent components correlating with a certain depth electrode contact are associated with a dipole located in close proximity to that contact. As a control, we also estimated the average Euclidean distance between the non-correlating components and all depth electrode contacts of a given patient. Given that we assume these non-correlating components to be associated with dipoles, located in various places in the brain that are not likely to be closer to the depth electrode contacts than the correlating components, a significant difference in localization accuracy for correlating and non-correlating dipoles would confirm our hypothesis. For the statistical analysis in this case, we used MATLAB to perform a linear mixed effect analysis of source localization accuracy (Gelman and Hill, 2006). We did this for ECoG data and EEG data separately. As a fixed effect, we used correlation and as random effects, we took frequency band, patients, modality, epoch length and depth electrode referencing montage:

$$source\ localization\ accuracy \sim correlation + (1|patient) + (1|frequencyband) + (1|epochlength) + (1|montage) \quad (1)$$

Finally, to compare the source localization accuracies of EEG and ECoG we used another linear mixed effect model to compare accuracy only between correlating dipoles of each modality. In this model, we took as fixed effect modality (EEG or ECoG) and as random effects frequency band, patient, epoch length and depth electrode referencing montage:

$$source\ localization\ accuracy \sim modality + (1|patient) + (1|frequencyband) + (1|epochlength) + (1|montage) \quad (2)$$

Furthermore, a similar pipeline analysis was performed similarly to the one described above, where bandpass filtering into the different frequency bands was omitted and data was filtered between 1-40 Hz. This pipeline and corresponding results can be found in the supplementary material, table S7 and the accompanying text (eq. S1 and eq S2).

4. Results

4.1. Activity from deep sources contribute to ECoG and EEG signals

Our first goal was to verify whether activity from deep sources spread to the cortical surface and scalp. Correlation analysis reveals a weak but significant ($rho_{average}$=0.13 (std=0.085), $p_{average}$=0.017 for all subjects and frequency bands, both ECoG and EEG) dependence between the depth electrodes and several subdural and scalp contacts. The correlation is significant and peaks at zero-lag, indicating that the relationship is not due to active transmission in neural pathways. Fig. 3 shows the zero-lag correlations for a single patient (patient P2) in the theta range, for 15 second long epochs (rho=0.18, p=0.0039 adjusted for multiple comparisons using FDR correction) when using a common average reference. Correlation values in the theta and alpha band are on average twice as large as in the beta band, for both ECoG and EEG. Table 1 shows

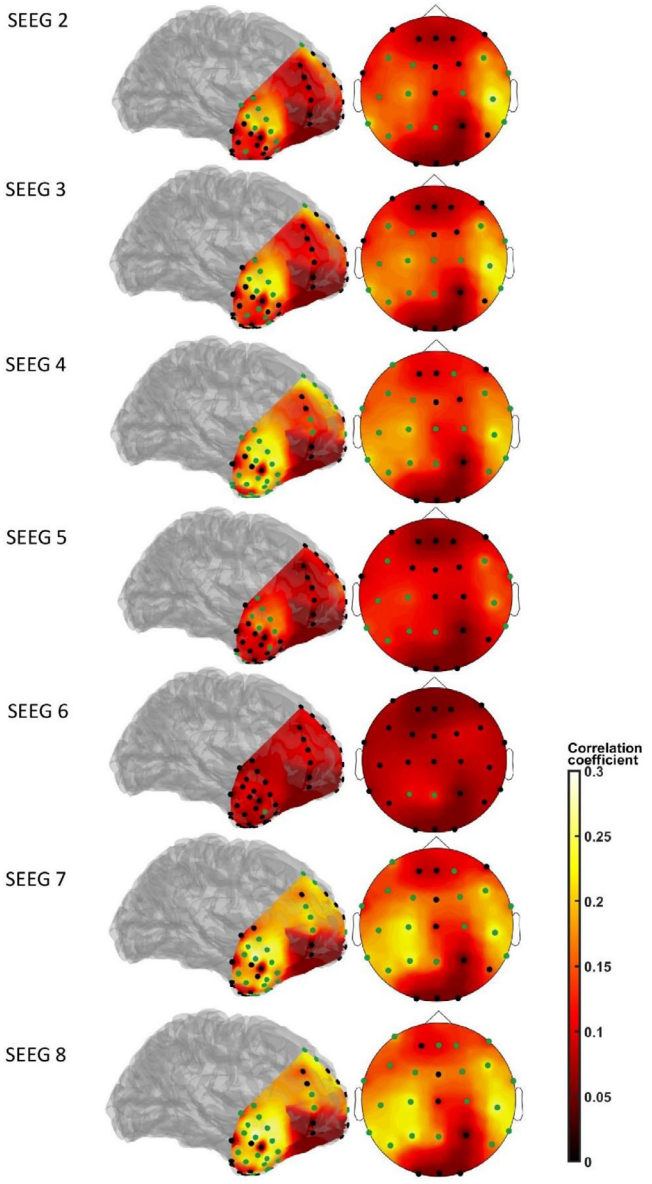

Fig. 3. Zero-lag correlation for each of the depth electrode contacts of patient P2 in theta band with ECoG (left column, left), and EEG (right column, right) sensors. Electrodes with significant correlation (FDR corrected) are marked in green.

Table 1.
Average correlation value of EEG/ECoG time series with depth electrode contacts across subjects per frequency band, for ECoG and EEG. P-values are adjusted for multiple comparisons using FDR correction.

Rho (p, FDR corrected)	theta	alpha	beta
ECoG	0.27 (p=0.011)	0.16 (p=0.015)	0.09 (p=0.02)
EEG	0.16 (p=0.010)	0.12 (p=0.020)	0.08 (p=0.023)

the average correlation across subjects. Additionally, Table S2 in supplementary material shows the correlation for each patient separately. This table shows a higher correlation value for P4 compared to other patients, which may have to do with the fact that P4 is the only patient where ECoG contacts cover both hemispheres.

As each EEG and ECoG electrode captures a mixture of signals originating from different sources, we applied ICA in an effort to single them

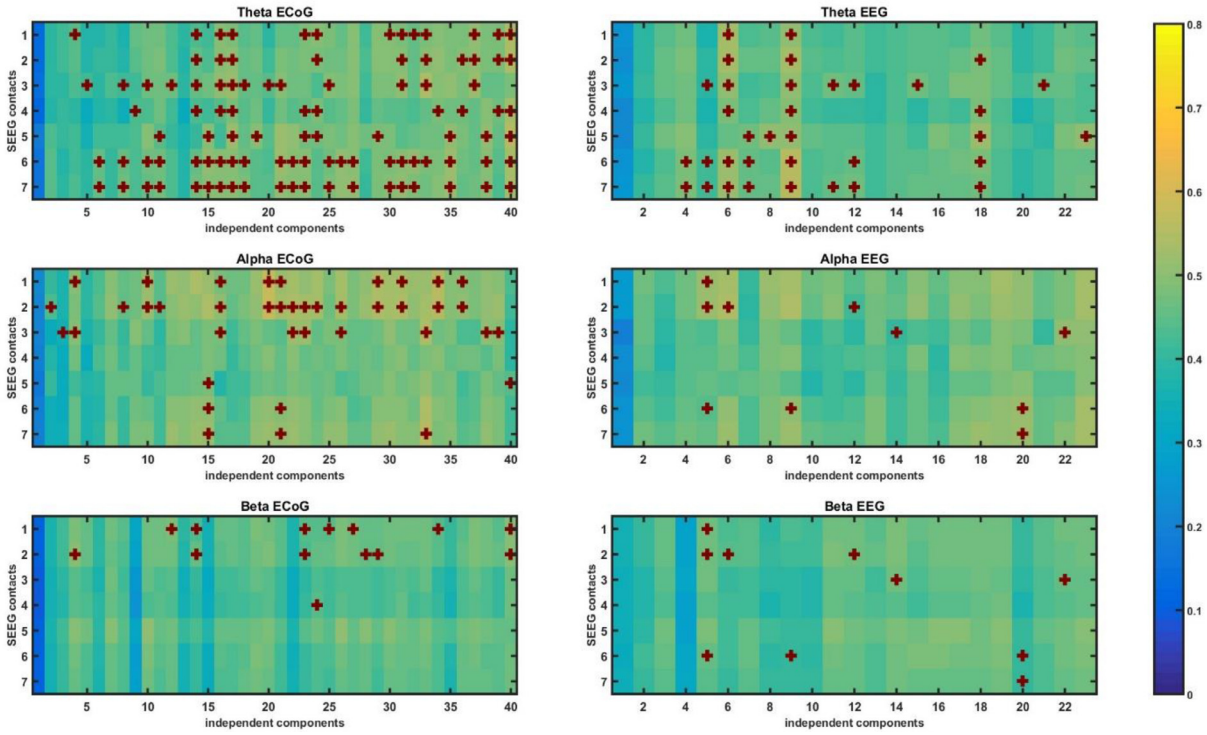

Fig. 4. Correlation values for ECoG and EEG in different frequency bands for patient 2. Significant values are marked by "+" (p-values are FDR corrected for multiple comparisons).

out (individual source contributions are further termed 'components'). We performed the ICA analysis as described in Materials and Methods and Fig. 2. In order to investigate the effect of different references for the depth electrodes, we analyzed our data using both the common average and bipolar re-referencing (see the section on pre-processing for a discussion). When using an average reference, a correlation analysis of the obtained components with respect to the (non-decomposed) depth electrode signals reveals, for all patients, components that significantly correlate with an average of 1.8 and 2.8 depth electrode contacts for the decomposed scalp- and subdural EEG, respectively (for a bipolar reference montage, these values correspond to 1.3 and 1.9, respectively). By contrast, a single depth electrode contact usually correlated with an average of 2.2 and 6 independent components for scalp and subdural EEG, respectively (bipolar: 2.2 and 5.8). A high number of subdural independent components are associated with the same depth electrode contact. This is similar to what was observed in previous studies (Whitmer et al., 2010). There, ICA analysis of ECoG data revealed multiple components that could be clinically identified as exhibiting frontal intermittent delta activity, therefore, the pathological brain signal could be represented by multiple independent components. In our case, it could be explained by the fact that depth electrode contacts record signals that are a combination of surrounding activity. Furthermore, in our study on average 24% of the scalp- and 39% of subdural components had a significant correlation with a given depth electrode contact (bipolar: 25% and 37.6%). Likewise, 48% and 76% of the total number of depth electrode contacts were significantly correlated with a given component (bipolar: 46.9% and 62.5%). A detailed list specific for each frequency band and epoch length is given in supplementary table S4 (and for the same analysis when using bipolar reference montage in table S5). Interesting to note here is that, there was no observed relationship between the number of depth electrode contacts correlating with a single IC and the median distance between depth electrode contacts and subdural electrodes in the patients (see also Table 3). The above-mentioned results are presented on a single subject level as follows: Fig. 4 shows for patient P2 significant correlations between independent components of ECoG and EEG and depth electrode contact activity in the theta band when taking epoch lengths of 15 seconds. The figures for the other patients along with those for the bipolar reference can be found in supplementary material figure S3. An average of the significant correlation values and their variance for each patient can also be found in supplementary table S3.

4.2. *Sources are more accurately localized from subdural than from scalp electrodes*

Each ICA component is believed to originate from an individual source in the brain (Delorme et al., 2012), see materials and methods section dipole modeling for a discussion). To identify the location of this source, each ICA component was subjected to a source localization analysis. After dipole fitting, dipoles with a goodness of fit above 75% were further analyzed in terms of source localization accuracy (as defined in materials and methods). For a single subject, we represent the results as follows: Fig. 5 shows the position, topography and time course of the independent component analysis for P2 in the theta band, for the three of the dipoles that had the best goodness of fit. Further information on the correlation values and accuracy of source localization for these specific dipoles can be found in Table 2. It should be noted that we also looked into the quality of the IC map for the ECoG grid. According to Whitmer et al. (2010), IC maps can be classified as "focal", or "diffuse" based on how the IC projects to the electrodes. A projection to two electrodes or less is considered to be "focal", whereas a projection to more than two contiguous electrodes is classified as "diffuse". Based on this definition, dipole 1 and 2 for the ECoG correspond to diffuse maps, as they both project to three contiguous electrodes, whereas dipole 3 projects to 2 electrodes and is, therefore, a focal map. In addition to the ECoG and EEG data, the location of the depth electrodes and their time course in the theta band for the same patient is shown in Fig. 6. A similar analysis for the theta, alpha and beta frequency bands of all subjects can be found in figure S4 of the supplementary material.

The source localization accuracy on population-level, for all epoch lengths, frequency bands and types of reference was statistical analyzed

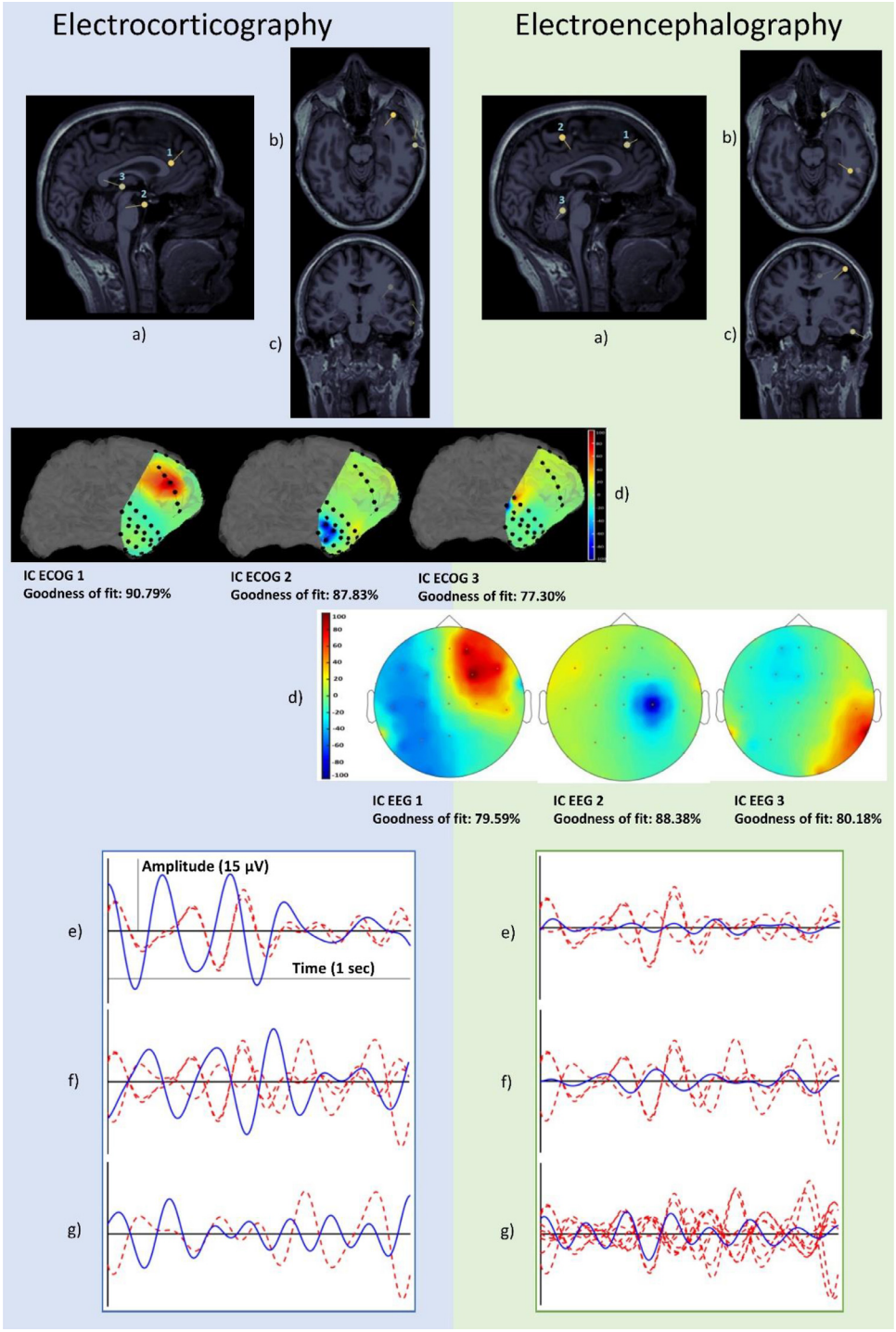

Fig. 5. Location of the three dipoles with the best goodness of fit in the theta band for patient 2, for d) ECoG and EEG in a) sagittal view, b) axial view, c) coronal view. d) topography of independent components, and e,f,g) 1 second time course of independent components 1, 2 and 3 for respectively ECoG and scalp EEG (shown in blue), with correlating time courses of the depth electrode contacts (shown in dashed red). Units for amplitude and time axis are shown in e) on the left.

using a linear mixed-effect model as described in Eqs. 1 and 2. Visual inspection of residual plots of all statistical models did not reveal any obvious deviation from normality. For within modality analysis of both ECoG and EEG, correlation affected source localization accuracy significantly with $P=2.898 \times 10^{-7}$ (estimate 0.0354, CI=[0.0219 0.0489], coefficient of determination $R^2=0.14$) for ECoG and $P=4.89 \times 10^{-4}$ (estimate 0.0273, CI=[0.012 0.0426], coefficient of determination $R^2=0.19$) for EEG, which indicates an improvement in source localization of around 3.54 and 2.73 cm for each modality. For the random effects, the linear mixed effect model returns an estimated covariance and its 95% confidence interval. The variation between random factors whose confidence interval did not include zero was not significant (see materials and methods, section on statistical analysis). This was the case for all random factors except for patients (estimate 0.0066, 0.0095, CI=[0.0034, 0.0127], [0.0091, 0.00099] for ECoG and EEG, respectively). Source localization analysis between modalities for significantly correlating dipoles showed a highly significant effect of reference type on modality (estimate 0.022, $P<10^{-12}$, CI=[0.025681, 0.0184], coefficient of determination $R^2=0.29$). This indicates an average source localization accuracy for EEG of 7.1 cm and for ECoG a significantly lower one of 4.9 cm. The variation between random effects was not significant. Fig. 7 shows a comparison of the source localization accuracy of ECoG and EEG. Residual plots for these results are given in supplementary figure S5. Results of the same statistical model for different values of dipole goodness of

Table 2.
Information complementary to figure 5. Listed are, for each IC correlating with a depth electrode contact and per modality: a) cross-correlation at zero-lag and b) source localization accuracy (cm).

	ECoG	EEG
IC1:	Contact 7: a) 0.4198 b) 6.08 Contact 8: a) 0.4974 b) 6.42	Contact 4: a) 0.3995 b) 7.13 Contact 7: a) 0.4379 b) 7.58 Contact 8: a) 0.4391 b) 7.88
IC2:	Contact 6: a) 0.4201 b) 4.10 Contact 7: a) 0.456 b) 4.19 Contact 8: a) 0.471 b) 4.46	Contact 6: a) 0.4191 b) 6.97 Contact 7: a) 0.4198 b) 6.65 Contact 8: a) 0.4274 b) 6.32
IC3:	Contact 6: a) 0.4912 b) 4.17	Contact 2: a) 0.3763 b) 4.7 Contact 3: a) 0.4015 b) 4.6 Contact 4: a) 0.3946 b) 4.04 Contact 5: a) 0.3819 b) 3.87 Contact 6: a) 0.4188 b) 3.54 Contact 7: a) 0.4525 b) 3.32 Contact 8: a) 0.4517 b) 3.1

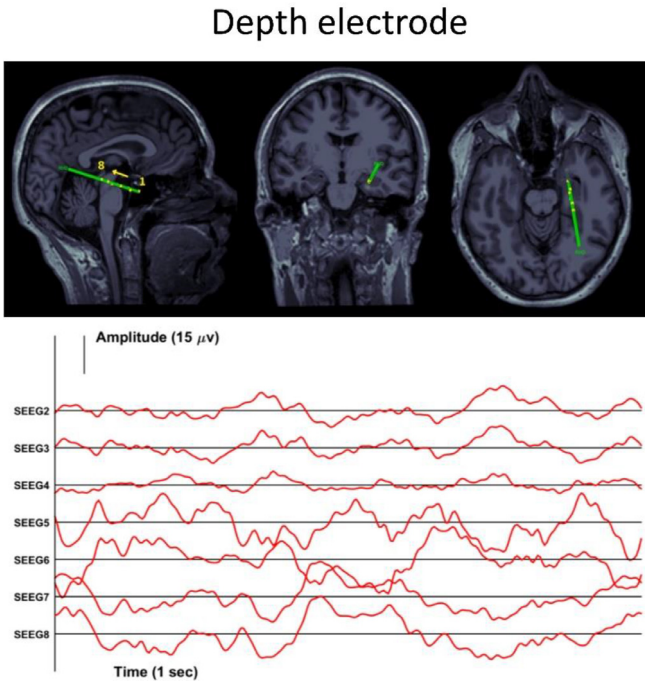

Fig. 6. Location and time series of depth electrode contacts for patient 2. Corresponding dipoles correlating with these times series can be found in fig. 5.

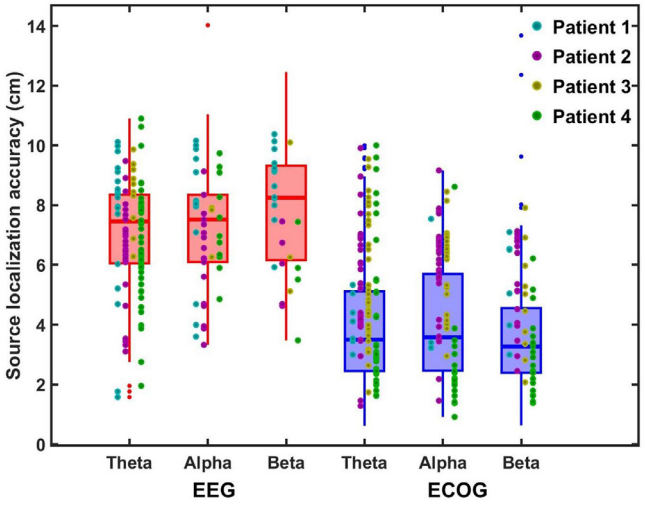

Fig. 7. Source localization accuracy (in meters) of ECoG and EEG, shown separately per frequency band. Colors of data points refer to patients.

fit are listed in supplementary table S6 (for the results of the broadband analysis, see supplementary table S7).

Since the effect of depth electrode reference was not significant, results shown from now on will be discussed based on average reference only (for both average and bipolar reference montage results, see supplementary material).

An overview of the distances between depth electrodes and ECoG and EEG electrodes, a short summary can be found in Table 3. As can be seen, the distance from depth electrodes to scalp electrodes is approximately twice the distance from depth electrodes to subdural grids.

5. Discussion

5.1. Simultaneous depth-ECoG-EEG recording allows for direct comparison of source localization accuracies

Our study aimed to quantitatively compare the localization accuracy of subcortical and deep sources from cortical ECoG and scalp EEG recordings. An initial analysis showed a small but significant correlation between depth electrodes and both ECoG and EEG. The fact that neural activity from depth electrode contacts could already be observed on both scalp and subdural electrodes before applying source separation techniques is an interesting finding as it supports a fair comparison of EEG and ECoG recordings in the detectability and localization accuracy of sources of neural activity.

Table 3.
Median distances between electrodes of the three modalities, for each patient.

Patient	Distance between Depth and EEG electrode (cm)	Distance between Depth and ECoG electrode (cm)
Patient 1	Median=10.5, sd=2.18	Median=5.2 sd=1.4
Patient 2	Median=10.3, sd=1.9	Median 4.2, sd=2
Patient 3	Median=10, sd=2	Median=5, sd=2.2
Patient 4	Median=10.8, sd=2.8	Median=3.4, sd=0.7

The ECoG and EEG signals were then each decomposed using ICA to isolate spatially distinct sources that contributed to the recorded signal. Our results showed that for both EEG and ECoG several independent components correlated with the (non-decomposed) signals at individual depth electrode contacts in the hippocampus or insula. The reconstructed sources based on these correlated components were located significantly closer to the depth contacts than their non-correlated counterparts.

Furthermore, our comparison between modalities confirmed a significant difference in source localization accuracy. When deep neural activity is detectable by EEG or ECoG we could locate this activity with an accuracy of 7.1 cm in EEG and 4.9 cm in ECoG. The poor performance of EEG source localization was to be expected given that, in addition to the limitations of the source localization model mentioned above, a minimum of 100 electrodes is required for a sufficiently accurate source localization (Liu et al., 2017) while in our case we had 27 active electrodes. Our results showed that for the same condition ECoG grids located in close proximity to the depth electrodes yielded an improved accuracy in the range of ~2 cm. It is interesting to note that while ECoG source localization performed indeed significantly better than EEG source localization on a population-level this was not significant on the scale of a single patient. Additionally, we believe that the improvement in source localization from EEG to ECoG of *deep sources* is not large enough to justify a preference for invasive measurement of ECoG over noninvasive EEG. Especially given that in simultaneous EEG/ECoG recording, there are several problems with source localization in scalp EEG, such as:

Due to the disruptive effect of the subdural grid on volume conduction, scalp activity was attenuated. Therefore, the minimum cortical extent needed to produce visible scalp activity can be overestimated (Ellenrieder et al., 2014, Lanfer et al., 2013). For example, a 4×8 grid can produce attenuation of 2 to 3 times, which means that the minimum cortical amplitude necessary to produce visible scalp activity is higher than when the subdural grid is absent (Ellenrieder et al., 2014).

1. The placement of the subdural grid and depth electrode was chosen to provide optimal visibility of the epileptic source. Therefore, even though the spatial coverage was limited, the subdural electrodes were placed quite close to the depth electrode. This is in contrast to the EEG electrodes, which were placed in a standard 10-20 international system whereby their position was not affected by the position of the depth electrode.

2. As previously stated, scalp electrodes were recorded from only 27 electrodes. Studies have shown for source localization accuracies in the range of 10~20mm, a minimum of 100 electrodes is required (Liu et al., 2017). This accuracy is likely even less for deep and subcortical sources.

3. Considering the unfavorable conditions of scalp electrodes mentioned above, we found an accuracy of 4.9cm for subdural grids vs. 7.1cm for EEG to be somewhat surprising. However, previous studies have already shown using computer simulations that EEG-based source localization in ideal conditions outperforms ECoG in cases where the strip and grid electrodes are not sufficiently close to the source of interest (Dümpelmann et al., 2009, Zhang et al., 2008). Our study showed that in deep structures, the distance between the deep source of neural activity and the ECoG grid does not allow for a very high source localization accuracy. It still remains to be seen how high-density EEG would perform in such a setting, but a recent study using simultaneous depth and high-density scalp EEG, during a very similar experimental condition, reported an accuracy of ~2cm (Seeber et al., 2019), emphasizing the impact of having more scalp electrodes, something much less expensive and risky than increasing the number of subdural electrodes. To the best of our knowledge, this was the first time these abovementioned claims were tested and investigated using real experimental data from human subjects when including a ground truth from the deep structures by means of depth electrodes.

We also investigated the variance caused by the two different types of referencing montage for the depth electrodes by including reference montage as a random factor in our statistical model. We found no effect of the choice of referencing (the 95% confidence interval of this variance did not exclude zero). Independent component analysis showed very similar results for both montages, as can be observed in supplementary tables S4 and S5 (for a summary, see Results section). Bipolar montages are presumed to be advantageous when attempting to pick up local activity as they help to cancel the more widespread activity. In our case, this cancellation effect did not differ from a common average montage of all depth electrode measuring sites. The reason for this could be explained as follows. Both types of reference are predominantly recording activity in the proximity of the depth electrode contact and the effect of a far source that propagates in a similar way to all depth electrodes will be canceled by both reference types (see supplementary material figure S6 for a simulation example). One should note that bipolar EEG also removes all signals common to the electrode pairs and that not all signals common to the electrode pairs come from the same reference. Hence, a given bipolar reference will completely miss dipoles with certain locations and tangential orientations (Hu et al., 2010). Geselowitz showed that if the model takes into account the positions of the sensors, the choice of a particular reference electrode does not in any way change the relation between source and potential, except for an additive constant of no physical significance (Geselowitz David, 1998). In conclusion, we do not believe the type of reference of the depth electrodes to have a substantial effect on the outcome of similar studies with simultaneous recordings of different modalities.

5.2. Controversy on detecting deep and subcortical activity from scalp and subdural EEG

Several studies have stated that at least $6cm^2$ of synchronous cortical activity is needed to generate a signal with a strong enough signal-to-noise ratio to be observed on the scalp without averaging (Nunez Paul and Srinivasan, 2006, Tao et al., 2005), although this has been called into question (Ramantani et al., 2016). While this statement suggests that unaveraged activity from smaller subcortical structures is not distinguishable from cortical activity, these structures still contribute considerably to scalp EEG and can be reliably localized under certain conditions. For example, in the case of brainstem evoked potentials, prior knowledge of the location and behavior of deep brain activity is available which causes subcortical activity of less than a microvolt to be detected (Picton and Terrence, 2010) and localized within the brainstem (Scherg and Von Cramon, 1985). Additionally, the suggested minimum area does not take into account that higher neural densities could produce the same amplitude within a smaller patch of tissue. It remains to be seen how the neural density of the human hippocampus compares to that of the neocortex. In rodents certain hippocampal structures with neural densities several times that of neocortical structures have been reported (Keller et al., 2018). Another concern might be that the distance

between the deep structures and the electrodes is weakening dipole contribution beyond observability as the amplitude of the electrical dipole decays as a function of distance, although this rate is very small for distances up to 10cm (Arnulfo et al., 2015, Scherg, 1990). Although the hippocampus is considered a deep structure, it is relatively superficial compared to subcortical structures. Indeed, the median distance between our depth electrode contacts located in the hippocampus was only 4.6cm for subdural grids and 11.9cm for scalp electrodes. Simulation studies suggest that source localization accuracy deteriorates beyond 6-8cm distance in ECoG (Pascarella et al., 2016) and for EEG it deteriorates gradually, at a constant rate (Whittingstall et al., 2003). Of course, while EEG is a complex signal, sensitive to both radial and tangential sources, and can more readily gauge potentials from deep sources in comparison to MEG, the signal-to-noise ratio of the activity attributed to these sources could still be potentially very low (Puce and S. Hämäläinen, 2017). Specifically, in recordings of spontaneous activity, the signal-to-noise ratio may be even poorer because of the overwhelming amount of simultaneously occurring activity. Indeed, our results showed that when independent component analysis was not used to increase the signal-to-noise ratio, correlations were very small (see Fig. 2) though still significant. In summary, more studies are presenting experimental and theoretical evidence suggesting the possibility to uniquely recover activity from both cortical and subcortical sources (Andersen et al., 2020, Attal et al., 2009, Attal and Schwartz, 2013, Krishnaswamy et al., 2017, Seeber et al., 2019).

5.3. Hippocampus at rest

The hippocampus plays a prominent role in central nervous system functioning. It can evoke large-scale influences on cortical activity, as it is a highly interconnected region, connected anatomically to a wide range of cortical regions (Cole et al., 2010). The contribution of hippocampal structures to scalp EEG and also MEG has recently become more accepted, as evidenced by deep structures such as the hippocampus for not being so “closed field” as previously thought, and therefore a cancellation of oppositely oriented dipole generators might not be as extensive (Attal et al., 2009, Attal and Schwartz, 2013, Meyer et al., 2017, Quraan Maher et al., 2011, Ruzich et al., 2019). Furthermore, experiments in mammals revealed subcortical structures such as the amygdala and thalamus to have a relatively high source density compared to the neocortex which is why in theory a smaller activated volume would be needed to produce a detectable signal on the scalp. This is also true for some parts of the hippocampus such as the dentate gyrus, although others have a lower current density (Keller et al., 2018). During rest, brain-wide slow oscillations are a characteristic feature of both the mammalian neocortex and the hippocampus occurring spontaneously and phase-locked to each other with a short delay (Chan et al., 2017, Wolansky et al., 2006). This suggests that, in low-frequency ranges, deep brain regions such as the hippocampus could initiate brain-wide cortical activity. Whether the hippocampal neural activity is picked up by subdural and scalp electrodes with sufficient signal-to-noise ratio to be visible is a question we have addressed in this study. In order to distinguish between the two likely types of activity propagation –physiological propagation of action potentials through causal interactions (active spread) and electrical volume conduction through cortical structures (passive spread) – timing is key. Therefore, for our investigation, it is crucial to eliminate correlations that were maximum at a non-zero lag. Future studies could look deeper into the phase relations between these types of activity propagation by using the imaginary part of phase-based connectivity techniques. However, even when controlling for zero-lag, we cannot fully rule out the possibility that activity from brain regions located outside the hippocampus is volume conducted at zero-lag to both depth electrodes and ECoG or EEG electrodes (Bénar and Badier, 2019). This is addressed further down under the limitations of the study, point III.

5.4. Detectability is more prominent for theta oscillations

Theta-alpha oscillations are prominently observed in the hippocampus of all mammals studied to date (Buzsáki, 2002). During quiet wakefulness, evidence exists for activity in the theta-delta range in the human hippocampus (Frauscher et al., 2018). Furthermore, it has recently been suggested that low-frequency hippocampal activity plays a significant role in defining the interhemispheric cortical resting-state connectivity and mediates visual processing. Our results show components correlating with a depth contact in the theta range twice as strong as correlating components in the alpha or beta range. This suggests the importance of slow-hippocampal activity in the formation of the electrophysiological signature of resting-state activity in the human brain (Chan et al., 2017).

5.5. Limitations of the study and suggestions for future research

On a final note, we want to point out the following practical and technical limitations of the current study as well as suggestions for future improvement:

While the topography of the scalp electrodes is in accordance with the standard 10-20 international system and common to all patients, the exact location and number of depth and subdural electrodes varies among patients (see supplementary material Table S1 and figure S1). This undeniably explains part of the observed variability.

The forward model currently provided in the Brainstorm toolbox does not account for surgery-induced effects, such as sutures of the skull and the impact of the non-conducting grid. Holes in the skull can have a large impact on the scalp potential distribution and neglecting them can lead to a systematic error in fitted source locations up to several centimeters (Oostenveld and (Oostenveld and F. Oostendorp, 2002)). Volume conduction models ignore such effects (Pascarella et al., 2016) although recently forward models have been developed for ECoG source localization in primates that take into account the implantation of very low conductivity ECoG silicone strips (Wang et al., 2019). However, in this study, our objective was not to achieve the best source localization accuracy, but rather to compare source localization between ECoG and EEG given the currently available models. In this respect, future studies are necessary to determine how much source localization with ECoG or EEG is affected by accounting for the above-mentioned issues. Furthermore, it would be of interest to investigate the neural activity of resting-state by means of methods that can combine EEG and ECoG withing a single head model. It still remains to be seen how such a model can improve the localization of deep brain structures, since previous simulations have shown little improvement in localization accuracy in areas beneath the non-conducting grid (Todaro et al., 2018).

In this study, we presumed independent components to have a significant zero-lag correlation with neural generators in close proximity to the depth electrode, though in theory, zero-lag correlation could be a result of distant coupled oscillators (Petkoski et al., 2018). We based our assertion on the observation that our independent components do not correlate with all depth contacts. If a neural generator would be located further away from the depth electrodes, most probably a correlation with the majority of the depth electrodes would be observed due to volume conduction. As far as we can see from tables S4 and S5, in most cases this does not happen, both for average and bipolar referencing of the depth electrode. Table S4 shows that, even in the subdural grids, the number of depth electrode contacts that correlate on average with a specific independent component is around 3 contacts (2.1 for bipolar reference) and rarely exceeds 5 contacts. Only in patient P2 (bipolar and average reference) and P4 (only average reference) did we find components that had a significant correlation with all depth electrode contacts in a hemisphere (see Figs. 4 and S3 in supplementary material). For patient P2, this was seen for one component in the theta band (same for bipolar) in both ECoG and EEG. For patient P4, 2 out of 16 subdural components in the theta and beta band were correlated with all depth electrode contacts (both hemispheres for the theta band,

only the right hemisphere for the beta band) and 4 out of 21 scalp components in the theta band showed significant correlation with all depth electrode contacts (2 of which were correlating with both hemispheres, one with left and one with the right hemisphere). Patient P4 also had the smallest distance between subdural and depth electrodes, which could explain the high number of correlated depth electrode contacts. In any case, the fact that this is not a common observation and that there is indeed a significant decrease in distance between the estimated dipoles and their correlated depth electrode contacts, compared to the average distance between the non-correlating dipoles and the average location of all depth electrode contacts, convinced us that correlating components are coming from neural generators in close proximity to the depth electrode contact. This presumption should be confirmed by studies for which there is prior knowledge of a neural generator located in deep or subcortical structures.

In this study, our method for source localization was restricted to dipole modeling. Future research is necessary to determine to what extent our results will be influenced when choosing alternative methods such as source distributed modeling (Jatoi Munsif et al., 2014).

Furthermore, recent studies have suggested the use of the Laplacian re-reference montage for depth electrodes as opposed to the bipolar and average montages used in this study (Li et al., 2019).

6. Conclusion

The assertion that deep structures such as the hippocampus do not produce activity visible on the scalp, due to their assumed “closed field” nature, is increasingly being challenged. Using a ground truth in the hippocampus and insula of 4 patients we showed that during quiet wakefulness, the activity picked up by depth electrodes indeed correlates with scalp EEG activity decomposed using ICA analysis. We speculate that these correlations stem from neural generators in close proximity to the depth electrodes for two reasons: I) an independent component was not observed by all depth electrodes and typically correlated with only a few of the depth electrode contacts, which hints at local activity and II) the result of dipole fitting for the correlated components showed a significant decrease in the distance between the dipole and depth electrode contact, compared to non-correlating components.

Furthermore, by simultaneously recording not only ECoG and scalp EEG but also depth electrodes, we were in a unique position to compare source localization accuracy of deep sources using invasive and non-invasive EEG. To the best of our knowledge, this is the first study presenting experimental findings on the comparison of invasive and non-invasive EEG source localization accuracy of deep cortical structures. Our results showed that, while source localization using invasive EEG turned out to be indeed significantly more accurate than using non-invasive EEG, we believe this improved accuracy is not satisfactory given that: I) scalp EEG is recorded with a low number of electrodes and partially shielded by the non-conducting ECoG grid, and II) the location of both ECoG electrodes and depth electrodes were chosen for optimal visibility and proximity to the epileptic source and were therefore in close proximity to each other.

7. Data availability

The datasets for this manuscript are not publicly available as it contains sensitive information about the patients and therefore cannot be transferred using online repositories.

Acknowledgments

The authors would like to thank Robert Oostenveld for his valuable input on the design of the study and the writing of the manuscript. MFH is supported by the Hermes Fund of the National Fund for Scientific Research Flanders (SB/151022). BW is supported by a postdoctoral mandate (PDM/19/176) from KU Leuven. EK is supported by the special research fund of the KU Leuven (C24/18/098). AL is supported by the Research Foundation Flanders (FWO 1SC3419N). EC, ID, AM and PB are supported by the Belgian Fund for Scientific Research – Flanders (G0A4118N). MMVH is supported by research grants received from the European Union’s Horizon 2020 research and innovation programme under grant agreement No. 857375, the Financing Program (PFV/10/008) and the special research fund of the KU Leuven (C24/18/098), the Belgian Fund for Scientific Research – Flanders (G088314N, G0A0914N, G0A4118N), the Interuniversity Attraction Poles Programme – Belgian Science Policy (IUAP P7/11), and the Hercules Foundation (AKUL 043).

Supplementary materials

Supplementary material associated with this article can be found, in the online version, at doi:10.1016/j.neuroimage.2020.117344.

References

Abraham, K., Ajmone Marsan, C., 1958. Patterns of cortical discharge and their relation to routine scalp electroencephalography. Electroencephalogr. Clin. Neurophysiol. 10 (3), 447–461.

Andersen, L.M., Jerbi, K., Dalal, S.S., 2020. Can EEG and MEG detect signals from the human cerebellum? NeuroImage 215, 116817. doi:10.1016/j.neuroimage.2020.116817.

Arnulfo, Gabriele, Hirvonen, Jonni, Nobili, Lino, Palva, Satu, Matias Palva, J., 2015. Phase and amplitude correlations in resting-state activity in human stereotactical EEG recordings. NeuroImage 112, 114–127.

Attal, Y., Bhattacharjee, M., Yelnik, J., Cottereau, B., Okada, Y., Lefevre, J., Bardinet, E., Chupin, M., Baillet, S., 2009. Modelling and detecting deep brain activity with MEG and EEG. IRBM 30 (3), 133–138.

Attal, Yohan, Schwartz, Denis, 2013. Assessment of subcortical source localization using deep brain activity imaging model with minimum norm operators : A MEG study. PLoS ONE 8 (3), e59856.

Ball, Tonio, Demandt, Evariste, Mutschler, Isabella, Neitzel, Eva, Mehring, Carsten, Vogt, Klaus, Aertsen, Ad, Schulze-Bonhage, Andreas, 2008. Movement related activity in the high gamma range of the human EEG. NeuroImage 41 (2), 302–310.

Ball, Tonio, Kern, Markus, Mutschler, Isabella, Aertsen, Ad, Schulze-Bonhage, Andreas, 2009. Signal quality of simultaneously recorded invasive and non-invasive EEG. NeuroImage 46 (3), 708–716.

Bénar, Christian-G., Badier, Jean-Michel, 2019. Simultaneous recordings of MEG and intracerebral EEG. In: Supek, E., Aine., C.J. (Eds.), Magnetoencephalography: From Signals to Dynamic Cortical Networks. Springer International Publishing, pp. 279–292.

Buzsáki, György, 2002. Theta oscillations in the hippocampus. Neuron 33 (3), 325–340.

Cebolla, A.M., Petieau, M., Dan, B., Balazs, L., McIntyre, J., Cheron, G., 2016. Cerebellar contribution to visuo-attentional alpha rhythm: insights from weightlessness. Sci. Rep. 6 (November), 37824.

Chan, Russell, W, Leong, Alex T.L., Ho, Leon C., P. Gao, Patrick, C. Wong, Eddie, M. Dong, Celia, 2017. Low-frequency hippocampal – cortical activity drives brain-wide resting-state functional MRI connectivity. In: Proceedings of the International Joint Conference on Neural Networks, 114, pp. E6972–E6981.

Cho, Jae-hyun, Hong, Seung-B., Jung, Young-Jin, Kang, Hoon-Chul, Kim, Heung-D., Suh, Minah, Jung, Ki-Young, Im, Chang-Hwan, 2011. Evaluation of algorithms for intracranial EEG (IEEG) source imaging of extended sources : feasibility of using IEEG source imaging for localizing epileptogenic zones in secondary generalized epilepsy. Brain Topogr. 24 (2), 91–104.

Cole, Michael, W., Pathak, Sudhir, Schneider, Walter, 2010. Identifying the brain’s most globally connected regions. NeuroImage 49 (4), 3132–3148.

Cosandier-rimélé, D., Bartolomei, F., Merlet, I., Chauvel, P., Wendling, F., 2012. Recording of fast activity at the onset of partial seizures : depth EEG vs . scalp EEG. NeuroImage 59 (4), 3474–3487.

Dalal Sarang, S., Baillet, Sylvain, Adam, Claude, Ducorps, Antoine, Schwartz, Denis, Jerbi, Karim, Bertrand, Olivier, Garnero, Line, Martinerie, Jacques, Lachaux, Jean-philippe, 2009. Simultaneous MEG and intracranial EEG recordings during attentive reading. NeuroImage 45 (4), 1289–1304.

Dale Anders, M., Fischl, Bruce, I. Sereno, Martin, 1999. Cortical surface-based analysis I. Segmentation and surface reconstruction. NeuroImage 9, 179–194.

Daly, Ian, Williams, Duncan, Hwang, Faustina, Kirke, Alexis, Eduardo R., Miranda, J. Nasuto, Slawomir, 2019. Electroencephalography reflects the activity of sub-cortical brain regions during approach- withdrawal behaviour while listening to music. Sci. Rep. 9 (9415), 1–22.

Delorme, Arnaud, Makeig, Scott, 2004. EEGLAB: an open source toolbox for analysis of single-trial EEG dynamics including independent component analysis. J. Neurosci. Methods 134 (1), 9–21.

Delorme, Arnaud, Palmer, Jason, Onton, Julie, Oostenveld, Robert, Makeig, Scott, 2012. Independent EEG sources are dipolar. PLoS ONE 7 (2), e30135.

Dubarry, Anne-sophie, Badier, Jean-michel, Fonseca, Agnès Trébuchon-da, Gavaret, Martine, Carron, Romain, Bartolomei, Fabrice, Liégeois-chauvel, Catherine, Régis, Jean, Chauvel, Patrick, Alario, F., Bénar, Christian, 2014. Simultaneous recording of MEG, EEG and intracerebral EEG during visual stimulation: from feasibility to single-trial analysis. NeuroImage 99, 548–558.

Dubey X, Agrita, Supratim Ray, X., 2019. Cortical electrocorticogram (ECoG) is a local signal. J. Neurosci. 39 (22), 4299–4311.
Dumas, Thibaud, Dubal, Stephanie, Attal, Yohan, Chupin, Marie, Jouvent, Roland, Morel, Shasha, George, Nathalie, 2013. MEG evidence for dynamic amygdala modulations by gaze and facial emotions. PLoS ONE 8 (9), 1–11.
Dümpelmann, Matthias, Fell, Jürgen, Wellmer, Jörg, Urbach, Horst, Christian E, Elger, 2009. 3D source localization derived from subdural strip and grid electrodes: a simulation study. Clin. Neurophysiol. 120 (6), 1061–1069.
Ellenrieder, Nicolás-Von, Beltrachini, Leandro, Carlos H, Muravchik, Gotman, Jean, 2014. Extent of cortical generators visible on the scalp : effect of a subdural grid. NeuroImage 101, 787–795.
Frauscher, Birgit, Von Ellenrieder, Nicolas, Zelmann, Rina, Dolez, Irena, Hall, Jeffery, Hoffmann, Dominique, Nguyen, Dang-Khoa, Minotti, Lorella, Kahane, Philippe, 2018. Atlas of the normal intracranial electroencephalogram: neurophysiological awake activity in different cortical areas. Brain 141 (4), 1130–1144.
Gelman, Andrew, Hill, Jennifer, 2006. Data Analysis Using Regression and Multilevel/Hierarchical Models. Cambridge University Press, New York.
Geselowitz David, B., 1998. The zero of potential. IEEE Eng. Med. Biol. 17 (1), 128–136.
Gharib, Sina, W. Sutherling, William, Nakasato, Nobukazu, S. Barth, Daniel, Baumgartner, Christoph, Alexopoulos, N., Taylor, Steve, L. Rogers, Robert, 1995. MEG and ECoG localization accuracy test. Electroencephalogr. Clin. Neurophysiol. 94, 109–114.
Gramfort, Alexandre, Papadopoulo, Théodore, Olivi, Emmanuel, Clerc, Maureen, 2010. OpenMEEG: opensource software for quasistatic bioelectromagnetics. Biomed. Eng. Online 9 (1), 45.
Grech, Roberta, Cassar, Tracey, Muscat, Joseph, Kenneth P, Camilleri, Fabri, Simon, Zervakis, Michalis, Xanthopoulos, Petros, Sakkalis, Vangelis, Vanrumste, Bart, 2008. Review on solving the inverse problem in EEG source analysis. J. NeuroEng. Rehab. 5 (1), 25.
Groppe David, M., Bickel, Stephan, J. Keller, Corey, K. Jain, Sanjay, T. Hwang, Sean, Harden, Cynthia, D. Mehta, Ashesh, 2013. Dominant frequencies of resting state human brain activity as measured by the electrocorticogram. NeuroImage 79, 223–233.
Haufe, Stefan, Deguzman, Paul, Henin, Simon, Arcaro, Michael, Christopher J, Honey, Hasson, Uri, C. Parra, Lucas, 2018. Elucidating relations between FMRI, ECoG, and EEG through a common natural stimulus. NeuroImage 179 (June), 79–91.
Himberg, Johan, Hyvarinen, Aapo, Esposito, Fabrizio, 2004. Validating the independent components of neuroimaging time series via clustering and visualization. NeuroImage 22 (3), 1214–1222.
Hu, Sanqing, Stead, Matt, Dai, Qionghai, Gregory A, Worell, 2010. On the Recording Reference Contribution to EEG Correlation, Phase Synchrony, and Coherence. IEEE Transactions on Systems, Man, and Cybernetics, Part B (Cybernetics) 40 (5), 1294–1304.
Huiskamp, G.J.M., 2002. Inverse and forward modeling of interictal spikes in the EEG, MEG and ECoG. In: Proceedings of the Second Joint 24th Annual Conference and the Annual Fall Meeting of the Biomedical Engineering Society][Engineering in Medicine and Biology, 2. IEEE, pp. 1393–1394.
Jatoi Munsif, Ali, Kamel, Nidal, Saeed Malik, Aamir, Faye, Ibrahima, Begum, Tahamina, 2014. A survey of methods used for source localization using EEG signals. Biomed. Signal Process. Control 11, 42–52.
Keller, Daniel, Erö, Csaba, Markram, Henry, 2018. Cell densities in the mouse brain : a systematic review. Front. Neuroanatomy 12 (October).
Koessler, Laurent, Cecchin, Thierry, Colnat-Coulbois, Sophie, Vignal, Jean-pierre, Jonas, Jacques, Vespignani, Herve, Ramantani, Georgia, Maillard, Louis-Georges, 2015. Catching the invisible : mesial temporal source contribution to simultaneous EEG and SEEG recordings. Brain Topogr. 28, 5–20.
Krishnaswamy, Pavitra, Obregon-Henao, Gabriel, Ahvenin, Jyrki, Khan, Sheraz, Babadi, Behtash, Iglesias, Juan-Egenio, S. Hämäläinen, Matti, L. Purdon, Patrick, 2017. Sparsity enables estimation of both subcortical and cortical activity from MEG and EEG. Proc. Natl. Acad. Sci. 114 (48), E10465–E10474.
Lanfer, Benjamin, Roer, Christian, Scherg, Michael, Rampp, Stefan, Kellinghaus, Christoph, Wolters, Carsten, 2013. Influence of a silastic ECoG Grid on EEG / ECoG based source analysis. Brain Topogr. 212–228.
Li, Guangye, Jiang, Shize, E. Paraskevopoulou, Sivylla, Wang, Meng, Xu, Yang, Zehan, Wu, Liang, Chen, Zhang, Dingguo, Schalk, Gerwin, 2019. Optimal referencing for stereo–electroencephalographic (SEEG) recordings. NeuroImage 183, 327–335.
Litvak, Vladimir, Eusebio, Alexandre, Jha, Ashwani, Oostenveld, Robert, R. Barnes, Gareth, D. Penny, William, Zrinzo, Ludvic, I. Hariz, Marwan, Limousin, Patricia, J. Friston, Karl, Brown, Peter, 2010. Optimized beamforming for simultaneous MEG and intracranial local field potential recordings in deep brain stimulation patients. NeuroImage 50 (4), 1578–1588.
Liu, Quanying, Farahibozorg, Seyedehrezvan, Porcaro, Camillo, Wenderoth, Nicole, Mantini, Dante, 2017. Detecting large-scale networks in the human brain using high-density electroencephalography. Hum. Brain Mapp. 38 (9), 4631–4643.
Marinazzo, Daniele, Riera, Jorge-J., Marzetti, Laura, Astolfi, Laura, Yao, Dezhong, Valdés, Pedro-A., 2019. Controversies in EEG source imaging and connectivity : modeling, validation, benchmarking. Brain Topogr. 32 (4), 527–529.
Meyer, S., Rossiter, Holly, Brookes, Matthew-J., Woolrich, Mark-W., Bestmann, Sven, Barnes, Gareth-R., 2017. Using generative models to make probabilistic statements about hippocampal engagement in MEG. NeuroImage 149 (June 2016), 468–482.
Musall, Simon, Von Pföstl, Veronika, Rauch, Alexander, K. Logothetis, Nikos, Whittingstall, Kevin, 2014. Effects of neural synchrony on surface EEG. Cereb. Cortex (April) 1045–1053.
Nunez Paul, L., D. Nunez, Michael, Srinivasan, Ramesh, 2019. Multi-scale neural sources of EEG: genuine, equivalent, and representative. A tutorial review. Brain Topogr. 32 (2), 193–214.
Nunez Paul, L., Srinivasan, Ramesh, 2006. Electric Fields of the Brain: The Neurophysics of EEG. Oxford university press.
Oostenveld, Robert, Fries, Pascal, Maris, Eric, Mathijs Schoffelen, Jan, 2011. FieldTrip: open source software for advanced analysis of MEG, EEG, and invasive electrophysiological data. Comput. Intell. Neurosci. 2011, 9.
Oostenveld, Robert, F. Oostendorp, Thom, 2002. Validating the boundary element method for forward and inverse EEG computations in the presence of a hole in the skull. Hum. Brain Mapp. 17 (3), 179–192.
Pascarella, A., Todaro, C., Clerc, M., Serre, T., Piana, M., 2016. Source modeling of Electro-CorticoGraphy (ECoG) data: stability analysis and spatial filtering. J. Neurosci. Methods 263, 134–144.
Pascual-Marqui, R.D.R.D., 1999. Review of methods for solving the EEG inverse problem. Int. J. Bioelectromagn. 1 (1), 75–86.
Petkoski, Spase, Matias Palva, J., K. Jirsa, Viktor, 2018. Phase-lags in large scale brain synchronization: methodological considerations and in-silico analysis. PLoS Comput. Biol. 14 (17), e1006160.
Picton Terrence, W., 2010. Human Auditory Evoked Potentials. Plural Publishing.
Pizzo, F., Roehri, N., Medina Villalon, S., Trébuchon, A., Chen, S., Lagarde, S., Carron, R., Gavaret, M., Giusiano, B., Mcgonigal, A., Bartolomei, F., Badier, J.M., Bénar, C.G., 2019. Deep brain activities can be detected with magnetoencephalography. Nat. Commun. 10 (971), 1–13.
Puce, Aina, S. Hämäläinen, Matti, 2017. A review of issues related to data acquisition and analysis in EEG/MEG studies. Brain Sci. 7 (58).
Quraan Maher, A., N. Moses, Sandra, Hung, Yuwen, Mills, Travis, J. Taylor, Margot, 2011. Detection and localization of hippocampal activity using beamformers with MEG : a detailed investigation using simulations and empirical data. Hum. Brain Mapp. 32, 812–827.
Ramantani, Georgia, Maillard, Louis, Koessler, Laurent, 2016. Correlation of invasive EEG and scalp EEG. Seizure: Eur. J. Epilepsy 41, 196–200.
Ruzich, Emily, Crespo-garcía, Maité, S. Dalal, Sarang, F. Schneiderman, Justin, 2019. Characterizing hippocampal dynamics with MEG: a systematic review and evidence-based guidelines. Hum. Brain Mapp. 40 (4), 1353–1375.
Samuelsson, John, G., Khan, Sheraz, Sundaram, Padmavathi, Peled, Noam, S. Hämäläinen, Matti, 2019. Cortical signal suppression (CSS) for detection of subcortical activity using MEG and EEG. Brain Topogr. 32 (2), 215–228.
Scherg, Michael, Von Cramon, Detlev, 1985. A new interpretation of the generators of BAEP waves I-V: results of a spatio-temporal dipole model. Electroencephalogr. Clin. Neurophysiol. 62, 290–299.
Scherg, Micheal, 1990. Fundamentals of dipole source potential analysis. Adv. Audiol. 6, 40–69.
Schoffelen, Jan-mathijs, Oostenveld, Robert, Fries, Pascal, 2008. Imaging the human motor system's beta-band synchronization during isometric contraction. NeuroImage 41, 437–447.
Seeber, Martin, Cantonas, Lucia-manuela, Hoevels, Mauritius, Sesia, Thibaut, Visser-vandewalle, Veerle, M. Michel, Christoph, 2019. Subcortical electrophysiological activity is detectable with high-density EEG source imaging. Nat. Commun. 10 (1), 753.
da Silva, Fernando, Lopes, H., 2011. Biophysical aspects of EEG and magnetoencephalogram generation. In: Schomer, D.L., da Silva, F.H.L (Eds.), Niedermeyer's Electroencephalography. Lippincott Williams & Wilkins, Philadelphia, pp. 91–110 edited by.
da Silva, Fernando, Lopes, H., 2019. Intracerebral sources reconstructed on the basis of high - resolution scalp EEG and MEG. Brain Topogr. 1–4.
Snyder, Adam C., Deepa, Issar, Smith, Mathew A., 2018. What does scalp electroencephalogram coherence tell us about long-range cortical networks? Eur. J. Neurosci. 48 (July 2017), 2466–2481.
Tadel, François, Baillet, Sylvain, C. Mosher, John, Pantazis, Dimitrios, M. Leahy, Richard, 2011. Brainstorm: a user-friendly application for MEG / EEG analysis. Comput. Intell. Neurosci. 8.
Tao, James-X., Ray, Amit, Hawes-ebersole, Susan, S. Ebersole, John, 2005. Intracranial EEG substrates of scalp EEG interictal spikes. Epilepsia 46 (5), 669–676.
Todaro, Chiara, Marzetti, Laura, A. Valdés Sosa, Pedro, A. Valdés, Pedro, Vittorio, Hernandez, 2018. Mapping brain activity with electrocorticography : resolution properties and robustness of inverse solutions. Brain Topogr. 0 (0), 0.
Todaro, Chiara, Marzetti, Laura, A. Valdés-Sosa, Pedro, A. Valdés-Hernandez, Pedro, Vittorio, Pizzella, 2019. Mapping brain activity with electrocorticography : resolution properties and robustness of inverse solutions. Brain Topogr. 32 (4), 583–598.
Tonoyan, Yelena, Chanwimalueang, Theerasak, P. Mandic, Danilo, M. Van Hulle, Marc, 2017. Discrimination of emotional states from scalp- and intracranial EEG using multiscale renyi entropy. PLoS ONE 12 (11), e0186916.
Tzovara, Athina, S. Meyer, Sofie, J. Bonaiuto, James, Abivardi, Aslan, R. Bach, Dominik, J. Dolan, Raymond, R. Barnes, Gareth, 2019. High-precision magnetoencephalography for reconstructing amygdalar and hippocampal oscillations during prediction of safety and threat. Hum. Brain Mapp. 2019, 1–16.
Wang, Qing, Valdés-hernández, Pedro-Antonio, Paz-linares, Deirel, Bosch-Bayard, Jorge, Oosugi, Naoya, Komatsu, Misako, Fuji, Naotaka, A. Valdés-Sosa, Pedro, 2019. EECoG–Comp : an open source platform for concurrent EEG / ECoG comparisons : applications to connectivity studies. Brain Topogr. 1–19.
Whitmer, Diane, Worrell, Gregory, Stead, Matt, Lee, Il-Keun, Makeig, Scott, 2010. Utility of independent component analysis for interpretation of intracranial EEG. Front. Hum. Neurosci. 4 (November), 1–13.
Whittingstall, Kevin, Stroink, Gerhard, Gates, Larry, Connolly, J.F, Finley, Allen, 2003. Effects of dipole position, orientation and noise on the accuracy of EEG source localization. Biomed. Eng. Online 2 (14), 1–5.
Wittevrongel, Benjamin, Khachatryan, Elvira, Fahimi, Mansoureh, Carrette, Evelien, De Taeye, Leen, Meurs, Alfred, Boon, Paul, Van Roost, Dirk, M. Van Hulle, Marc, 2018. Representation of steady-state visual evoked potentials elicited by luminance Fl Icker in human occipital cortex : an electrocorticography study. NeuroImage 175 (January), 315–326.

Wolansky, Trish, A. Clement, Elizabeth, R. Peters, Steven, A. Palczak, Michael, T. Dickson, Clayton, 2006. Hippocampal slow oscillation : a novel EEG state and its coordination with ongoing neocortical activity. J. Neurosci. 26 (23), 6213–6229.

Zhang, Yingchun, Drongelen, Wim-Van, Kohrman, Michael, He, Bin, 2008. Three-dimensional brain current source reconstruction from intra-cranial ECoG recordings. NeuroImage 42, 683–695.